

# Cosmic-Ray Events as Background in Imaging Atmospheric Cherenkov Telescopes

G. Maier<sup>1,2</sup> and J. Knapp<sup>1</sup>

<sup>1</sup>Department of Physics, McGill University, Montréal, Canada H3A 2T8\*

<sup>2</sup>School of Physics and Astronomy, University of Leeds, Leeds LS2 9JT, UK

October 29, 2018

## Abstract

The dominant background for observations of  $\gamma$ -rays in the energy region above 50 GeV with Imaging Atmospheric Cherenkov telescopes are cosmic-ray events. The images of most of the cosmic ray showers look significantly different from those of  $\gamma$ -rays and are therefore easily discriminated. However, a small fraction of events seems to be indistinguishable from  $\gamma$ -rays. This constitutes an irreducible background to the observation of high-energy  $\gamma$ -ray sources, and limits the sensitivity achievable with a given instrument. Here, a Monte Carlo study of  $\gamma$ -like cosmic-ray events is presented. The nature of  $\gamma$ -like cosmic-ray events, the shower particles that are responsible for the  $\gamma$ -like appearance, and the dependence of these results on the choice of the hadronic interaction model are investigated. Most of the  $\gamma$ -like cosmic ray events are characterised by the production of high-energy  $\pi^0$ 's early in the shower development which dump most of the shower energy into electromagnetic sub-showers. Also Cherenkov light from single muons can mimic  $\gamma$ -rays in close-by pairs of telescopes. Differences of up to 25% in the collection area for  $\gamma$ -like proton showers between QGSJet/FLUKA and Sibyll/FLUKA simulations have been found.

## 1 Introduction

The study of the non-thermal universe at energies above 80 GeV by means of ground-based  $\gamma$ -ray astronomy has evolved substantially in the past few years. About 40 sources of high energy  $\gamma$ -rays are known, including Pulsar Wind Nebula (e.g. the Crab Nebula), Supernova Remnants (e.g. RX J 1713.7-3946), Active Galactic Nuclei (e.g. Markarian 421), X-ray binaries (e.g. LS5039 [2]), our own galactic centre and even objects that are not seen in any other waveband (e.g. HESS J1614-518 [1]). This progress is due to the large increase in sensitivity of new instruments, which consist of arrays of large imaging atmospheric Cherenkov telescopes (IACT). These systems detect Cherenkov light from air showers simultaneously in several telescopes. The sensitivity increase is primarily due to the much improved suppression of the background of hadronic cosmic rays, which are more than a thousand times more numerous than the  $\gamma$ -rays.

Arrays of imaging atmospheric Cherenkov telescopes reject a significant number of cosmic rays already at the trigger level by requiring compact patterns (e.g. more than 3 adjacent pixels) in two or more telescopes. Further suppression is achieved by applying cuts to the shape parameters describing the images (i.e. the Cherenkov light distribution) in the focal plane. For point-like or slightly extended sources the reconstructed arrival direction can also be used to distinguish between  $\gamma$ -rays and the isotropic Cosmic-rays. The combination of all selection cuts leads to the elimination of the major part of the background events. For point-like sources, image shape and shower direction cuts typically suppress the background by a factor of 2000. Even so, after all

---

\*Phone: +1 514 398 6492, email: maierg@physics.mcgill.ca

$\gamma$ -hadron separation cuts, a small but significant fraction of the remaining events are of hadronic origin. The large ratio of cosmic rays to  $\gamma$ -rays and the substantial fluctuations in the shower development of hadronic showers lead in general to a considerable overlap of the distributions of shower parameters, which are used for the separation. Observations are therefore still background limited and most of the weaker known sources require observation times in the range of 10-80 hours for a significant detection. In general, even longer times are needed for morphology studies of extended objects, and for the detection of sources close to the sensitivity limit of the instrument. Many undetected sources are expected at fluxes just below the current sensitivity of about  $10^{-13} \text{ cm}^{-2} \text{ s}^{-1}$  and at energies between 20 and 250 GeV. Therefore, several groups are currently studying how to access these regions. Sensitivity improvements and the extension of the energy range to lower energies requires the collection of more Cherenkov photons at ground level and improved  $\gamma$ -hadron separation. The former can be achieved, for example, by increasing the size of the telescopes, by increasing the quantum efficiency of the cameras, or by building more telescopes. The latter relies on profound knowledge of the development of  $\gamma$ -ray and cosmic-ray initiated showers in the atmosphere, and requires an algorithm to identify the subtle differences between them. Both the improvement of current systems and the design of new observatories are studied with detailed Monte Carlo simulations of air shower development and instrument performance.

Unfortunately, it is an immense effort to simulate the background for current IACTs. Typically only about one in  $10^6$ - $10^7$  simulated proton showers triggers an array and passes all  $\gamma$ -hadron separation cuts. This makes background estimation with simulations, and systematic studies of telescope designs, trigger conditions, reconstruction procedures etc. very time-consuming.

In this paper we study background events in IACTs for two reasons: firstly, to understand the origin of  $\gamma$ -like cosmic ray showers (and perhaps to improve the  $\gamma$ -hadron separation in the data analysis), and secondly, to find a feature in the early shower development in order to distinguish between  $\gamma$ -like and other proton showers and to limit the simulation effort to the small fraction of showers which will finally pass all cuts.

The main characteristics of the simulations, the telescope array and the analysis method are presented in Section 2. A detailed study of  $\gamma$ -like background events is given in Section 3. Section 3.1 emphasizes the importance of the geometrical arrangement of the telescopes and introduces a cut against muon-induced background events for telescope pairs located close to each other. Section 3.2 describes why some of the background events are indistinguishable from  $\gamma$ -ray events and in Section 4 the differences due to different hadronic interaction models are discussed.

## 2 Simulations and analysis methods

Simulations and the subsequent data analysis have been carried out in several steps. The first step consists of the simulation of extensive air showers induced by primary protons and  $\gamma$ -rays and the Cherenkov light production by the shower particles. Next, the Cherenkov photons are tracked through the telescope optics and the camera response is modeled. Finally, the resulting telescope images are analyzed with commonly used methods, including a second-moment analysis of the shower images in the cameras [13] and the reconstruction of shower directions and impact parameters [20].

Extensive air showers induced by primary protons with energies following a power law with a differential spectral index of -2.7 between 50 GeV and 10 TeV are simulated with the CORSIKA code v.6.2 [9]. As more than 75% of all cosmic rays are protons in this energy range and arrays of IACTs are much less sensitive to air showers from heavier nuclei (at the same energy), only protons have been simulated (see as well section 3.2). The contribution from cosmic electrons has been neglected here. The energy threshold after analysis cuts of the considered telescope array is well above 100 GeV, where the cosmic electron flux is significantly below the background due to hadronic cosmic rays.

The isotropic arrival directions of cosmic rays are simulated by randomizing the shower directions in a cone with an opening angle of  $3.5^\circ$  around the vertical pointing direction of the telescopes. Shower cores are distributed randomly on a circular area with a radius of 600 m

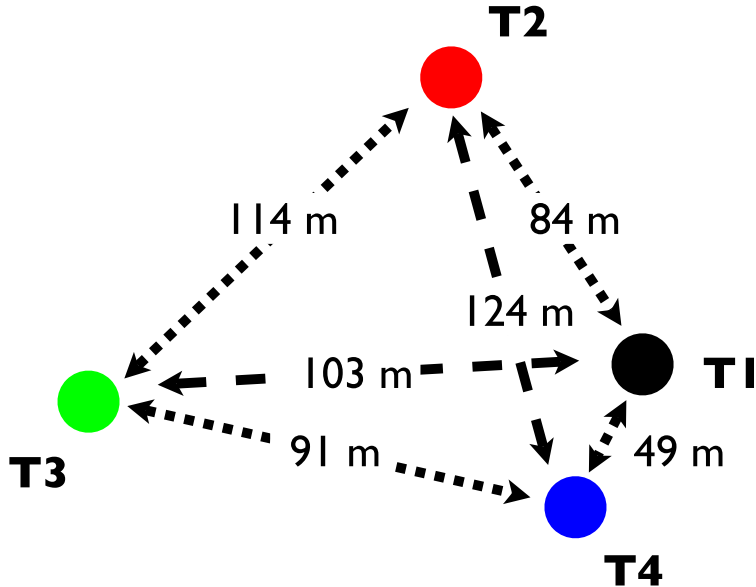


Figure 1: Layout of the array of imaging atmospheric Cherenkov telescopes used in this paper (similar to the temporary VERITAS layout).

around a point located roughly in the center of the array of telescopes. The parameters for the  $\gamma$ -ray simulations differ only in the differential spectral index (which is -2.5, similar to the energy spectrum of the Crab Nebula [14]) and the arrival directions, which are assumed to be from a point source. The shower simulations use the U.S. standard atmosphere [22] and atmospheric extinction values estimated with Modtran 4 [19], assuming 50 km visibility at ground level for a wavelength of 550 nm.

Two different combinations of low and high-energy interaction models are used: QGSJet (version 01c) [16] and FLUKA (version 2003.1) [7] with a transition energy of 500 GeV, and Sibyll (version 2.1) [6] and FLUKA (version 2003.1) with a transition energy of 80 GeV [12]. Calculation of all electromagnetic interactions are performed with EGS4 [23] which is well tested and has small uncertainties, even up to 100 TeV. Specifically, this is demonstrated by the good agreement between simulated and real  $\gamma$ -ray images that is usually achieved for Cherenkov telescope experiments (see e.g. ref. [21]). Approximately  $5 \times 10^8$  proton events have each been simulated for the QGSJet/FLUKA and Sibyll/FLUKA sets.

The array of IACTs consists of four telescopes arranged in a quadrangle with different sides (see Figure 1). The pointing direction of all telescopes is the same, namely directly towards the source. No convergent towards the shower maximum is used. All telescopes are at the same altitude of 1270 m above sea level. The telescopes are Davies-Cotton reflectors of 12 m diameter with a focal length of 12 m. Each reflector comprises 350 hexagonal mirror facets of a total area of 110 m<sup>2</sup>. The cameras are equipped with 0.15° diameter photomultiplier tubes (PMT) with characteristics similar to the Photonis XP2970 model in an hexagonal arrangement. Light cones are simulated which yield a geometrical collection efficiency of 85% for Cherenkov photons hitting the focal plane. The local trigger system consists of a simple multiplicity trigger of three adjacent PMTs with signals above a threshold of  $\approx 4$  p.e. in a time window of 5 ns. The array

trigger requires at least two telescopes with a local trigger in a time window of 100 ns.

The telescope simulation [5] consists of two parts, the propagation of Cherenkov photons through the optical system and the response of the camera and electronics. The signal in a PMT is created by summing up single photo-electron pulses with appropriate time and amplitude jitters. Night sky background light, electronic noise and all efficiencies, including mirror reflectivities, geometrical, quantum, and collection efficiencies, and losses due to signal transmission have been modeled. The design of the telescopes and their arrangement are similar to the temporary installation of the VERITAS array [26] at the Fred Lawrence Whipple Observatory in Southern Arizona, USA. The presented work was prepared during the construction phase of VERITAS and several changes in layout and design of the actual system made it impossible to compare in detail the simulations presented here with array data. The simulation chain has been extensively tested on single telescope data and reproduces the characteristics of the VERITAS-1 telescope [21].

The event reconstruction procedure consists of image cleaning, second-moment image analysis [13] for each camera, and reconstruction of shower direction and impact parameter on the ground, using all available images. Images are cleaned by removing pixels with signals of less than five and three times the noise variation for pixels near the centre and at the perimeter of the image, respectively. In the second moment analysis, the axes and widths of the image are determined. Images of at least five pixels are required for the array reconstruction. The intersection of the extrapolated long axes of the different images defines the shower direction [15].

Thus, events first have to fulfill a set of *event quality* conditions: at least 5 pixels per image, the moment analysis must be successful, and reconstruction of the shower direction and impact point must be possible.

The background rejection method consists of shape and direction cuts. Showers induced by cosmic rays usually have much broader and very irregular images in the camera, while showers induced by  $\gamma$ -rays have the shape of slim, elongated ellipses. Look-up tables containing the expected width and length for a given image size and distance of the telescope from the shower impact position ( $width_{expected}(R_i, size_i)$ ) are filled from simulated  $\gamma$ -ray showers. These tables are used to calculate the mean deviation in width and length of images in each camera from their expected values [3]. These mean values are generally called *mean scaled width* (MSCW) and *mean scaled length* (MSCL). MSCW is defined according to

$$MSCW = \frac{1}{N_{tel}} \times \left[ \sum_i^{N_{tel}} \frac{width_i - width_{expected}(R_i, size_i)}{\sigma_{width_{expected}}(R_i, size_i)} \right] \quad (1)$$

where  $N_{tel}$  is the number of telescopes with a good image,  $R_i$  is the distance of telescope  $i$  from the shower impact position,  $size_i$  is the total number of photoelectrons recorded in telescope  $i$ . An analogous formula is used to calculate mean scaled length. Figure 2 shows the significant difference between the MSCW distributions for  $\gamma$ -rays and protons.

The last important cut is on the direction of the incoming shower. Only events coming from the source direction are accepted as  $\gamma$ -rays. This is expressed through the variable  $\Theta^2$ , which describes the squared angular difference between source and reconstructed shower direction. Obviously this cut suppresses a significant part of the isotropic background, while retaining the source events. The better the angular resolution of the telescope array, the more restrictive this cut can be chosen.

The following  $\gamma$ -hadron selection cuts have been used: candidate events are accepted as  $\gamma$ -rays if  $MSCW < 0.3$ ,  $MSCL < 0.45$ , and  $\Theta^2 < 0.015 \text{ deg}^2$ . (To increase the number of  $\gamma$ -like proton events a much wider direction cut for proton events of  $\Theta^2 < 1 \text{ deg}^2$  is applied in the following. All results are then scaled to the opening angle of  $\Theta^2 < 0.015 \text{ deg}^2$ .)

Table 1 shows that only about one in seven million simulated proton showers passes the trigger and reconstruction requirement and the  $\gamma$ -hadron separation cuts (this value depends on the size of the scatter area). With the described  $\gamma$ -hadron selection cuts a hadron suppression factor of about 2000 relative to the number of reconstructed proton events is achieved. In contrast, one out of 200 simulated  $\gamma$ -rays passes these cuts, about 60% of all reconstructed  $\gamma$ -rays are lost in the process. The term  *$\gamma$ -like event* is used in the following for an event which passed all cuts described above.

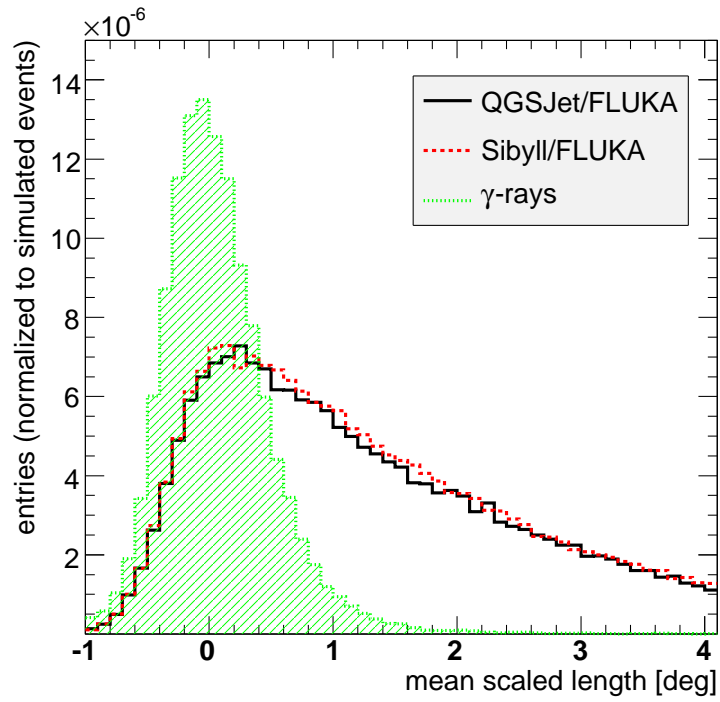


Figure 2: Mean scaled width distribution for events passed the trigger and reconstruction cuts. Primary  $\gamma$ -rays and protons are shown (QGSJet/FLUKA and Sibyll/FLUKA simulations).

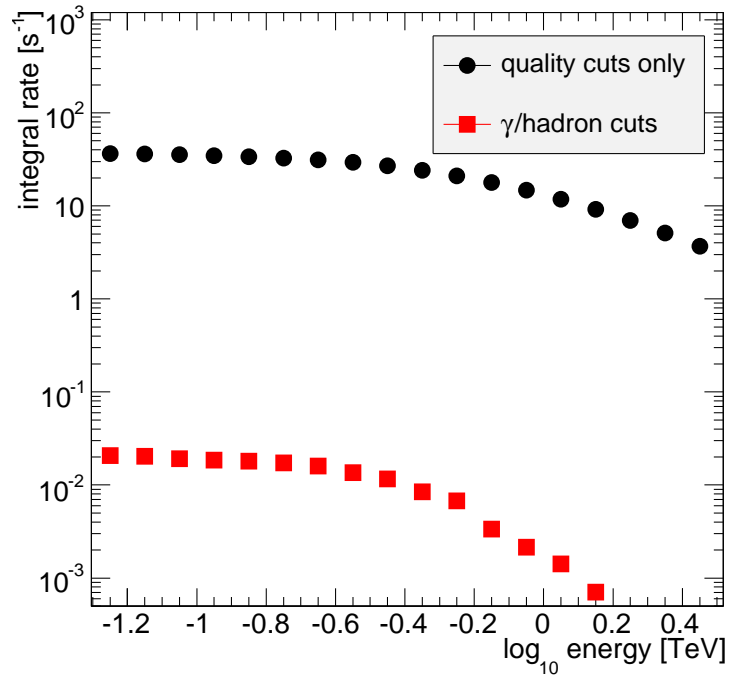


Figure 3: Integral rates of primary protons after quality cuts, and after  $\gamma$ -hadron separation cuts (QGSJet/FLUKA simulations).

Figure 3 shows the integral rates for protons for quality cuts only (at least 5 pixels per image, successful image parameterisation, and reconstruction of shower direction and impact point) and after  $\gamma$ /hadron separation cuts have been applied.

### 3 A closer look at $\gamma$ -like proton showers

The proton events which pass all  $\gamma$ -hadron separation cuts, described in the previous section, end inevitably in the  $\gamma$ -ray sample. It is known that the decay of high-energy neutral pions into two  $\gamma$ -rays in an early stage of the shower development is often the reason for proton showers to look like  $\gamma$ -ray showers (see e.g. [25]).

However, in our event sample we find a second class of  $\gamma$ -like events. These are events with high-energy muons ( $> \text{few GeV}$ ) near the array center. Cherenkov light emitted from these muons is usually confined to a much smaller area than Cherenkov light from air showers, but high local photon densities can trigger telescopes and display  $\gamma$ -like images. Due to the small lightpool of an energetic muon, multiple telescope images occur only if telescopes are close to one another. The array layout considered here, with distances between individual telescopes as small as 49 m, causes the relatively large sensitivity to such muonic events. Generally, distances between telescopes are much larger, in the range of 80 m (e.g. the future VERITAS array or MAGIC-II) to 120 m (e.g. H.E.S.S.), and consequently the muon sensitivity is reduced for those arrangements.

#### 3.1 Muonic $\gamma$ -like proton showers

The total number of Cherenkov photons emitted by a muon and their spatial distribution depends mainly on the muon energy (the number of Cherenkov photons  $N_C$  produced per path length  $s$  is  $dN_C/ds \propto \int \sin^2 \Theta_C / \lambda^2 d\lambda$ .  $\Theta_C$  describes the Cherenkov emission angle  $\cos \Theta_C = 1/(\beta n)$ ,  $\beta$  the muon velocity,  $n$  the refractive index, and  $\lambda$  the wavelength of the Cherenkov photons). Most of the light seen by the telescopes is produced within a few kilometers of ground level.

In proton showers of 50 GeV to 10 TeV, typical muon energies at ground level are between 1 and 20 GeV, but the muon energy distribution extends beyond several hundred GeV. These muons originate mainly from low-energy protons which produce only one or a few secondaries in a peripheral collision, which then produce one or a few muons, carrying most of the primary energy. The few other shower particles are absorbed at large heights, and almost no particles or Cherenkov photons reach the ground. Figure 4 (right) shows a typical muonic event which passed all  $\gamma$ -hadron separation cuts. Several circular Cherenkov light pools of about 120 m radius can be seen, corresponding to muon energies of roughly 50 GeV to 80 GeV. This muonic event triggered telescopes 1 and 4, which have the smallest distance to each other (49 m).

The role of Cherenkov light from muons was studied with a special set of simulations. All  $\gamma$ -like showers were simulated a second time, but with Cherenkov emission from muons now switched off. By comparing the two simulation sets event-by-event, the fraction of Cherenkov photons hitting a telescope which were produced by muons ( $=F_\mu$ ) could be determined.

$F_\mu$  is plotted for all  $\gamma$ -like proton events in Figure 5. The fraction of events with  $F_\mu < 0.5$  and  $F_\mu > 0.5$  are listed in Table 1.  $F_\mu > 0.5$  means that more than 50% of all Cherenkov photons recorded by the telescopes is emitted by muons. It is obvious that there are two classes of events and that muonic showers, i.e. showers with  $F_\mu > 0.5$  are only able to trigger two telescopes. In about 30% of all  $\gamma$ -like proton showers, Cherenkov photons from muons are the dominant part. Almost all of them are two-telescope events. Events with  $F_\mu > 0.5$  are called *muonic events* in the following.

The number of  $\gamma$ -like two-telescope events increases sharply with shrinking telescope distances due to the contribution of muons (Figure 6). The rate increase can be understood as the increase in the allowed region of impact points for muons with a given energy, and hence radius of Cherenkov light pool. The area of this allowed region is small or zero for small muon energies or large telescope distances. Figures 5 and 6 show that more than half of the  $\gamma$ -like muonic events are T1+T4 events, the pair with the smallest telescope distance (49 m).

		number of simulated events	fraction of reconstructed events	fraction of $\gamma$ -like events	$N_{tel} = 2$	$N_{tel} = 3$	$N_{tel} = 4$
QGSJet/FLUKA (proton simulations)	All events	$4.6 \cdot 10^8$	$3.3 \cdot 10^{-4}$	$1.5 \cdot 10^{-7}$	83%	13%	4%
	$F_\mu < 0.5$	-	-	70%	65%	99%	100%
	$F_\mu > 0.5$	-	-	30%	35%	1%	0%
Sibyll/FLUKA (proton simulations)	All events	$5 \cdot 10^8$	$3.4 \cdot 10^{-4}$	$1.5 \cdot 10^{-7}$	83%	13%	4%
	$F_\mu < 0.5$	-	-	72%	67%	99.5%	100%
	$F_\mu > 0.5$	-	-	28%	33%	0.5 %	0%
$\gamma$ -rays	All events	$5 \cdot 10^6$	$1.2 \cdot 10^{-2}$	$5 \cdot 10^{-3}$	6.9%	26.4%	66.7%

Table 1: Overview of number of simulated and reconstructed events, number of selected events, and fraction of events with telescope multiplicity 2, 3, and 4. Note that the rows for  $\pi^0$ -like ( $F_\mu < 0.5$ ) and muon-like events ( $F_\mu > 0.5$ ) quantify the number of 2, 3, or 4-telescope events as fraction of all events with the same number of telescopes. Selected events are events with MSCW  $< 0.35$ , MSCL  $< 0.45$ , and  $\Theta^2 < 0.015 \text{ deg}^2$ .

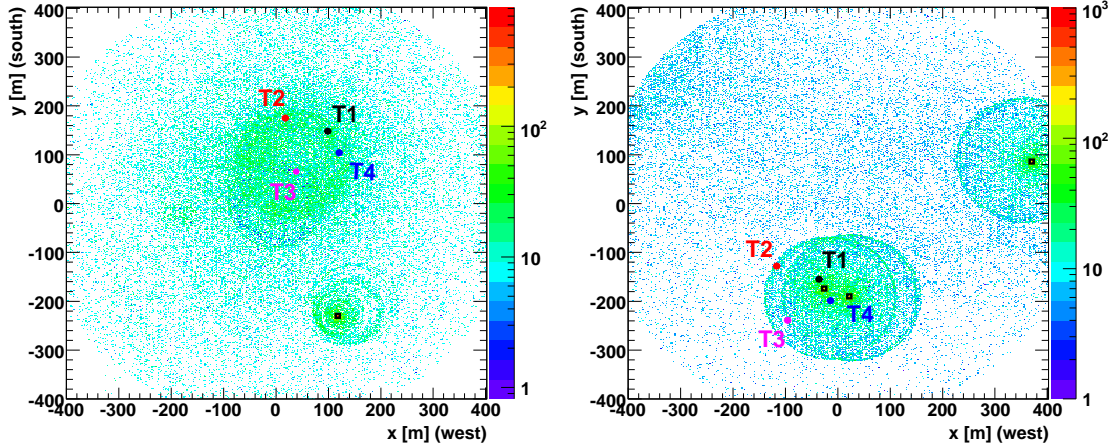


Figure 4: Cherenkov photon distributions at ground for two typical  $\gamma$ -like events. The color scale indicates the number of Cherenkov photons per bin. left: telescopes triggered by pionic subshower. right: telescopes triggered by muon rings. The position of the four telescopes are indicated by small circles (T1: black, T2: red, T3: green, T4: blue). High-energy muons ( $E_\mu > 5 \text{ GeV}$ ) are drawn as small black squares. Only Cherenkov photons with distances smaller than 450 m to the position of the shower core are shown. (QGSJet/FLUKA simulations)

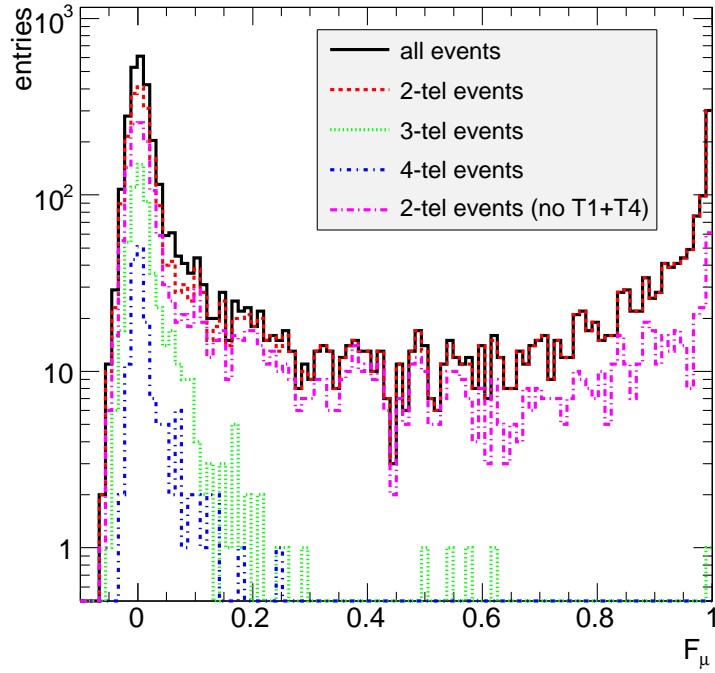


Figure 5: Distribution of the fraction of measured Cherenkov light emitted by muons ( $F_\mu$ ) in  $\gamma$ -like events for different telescope multiplicities (QGSJet/FLUKA simulations).

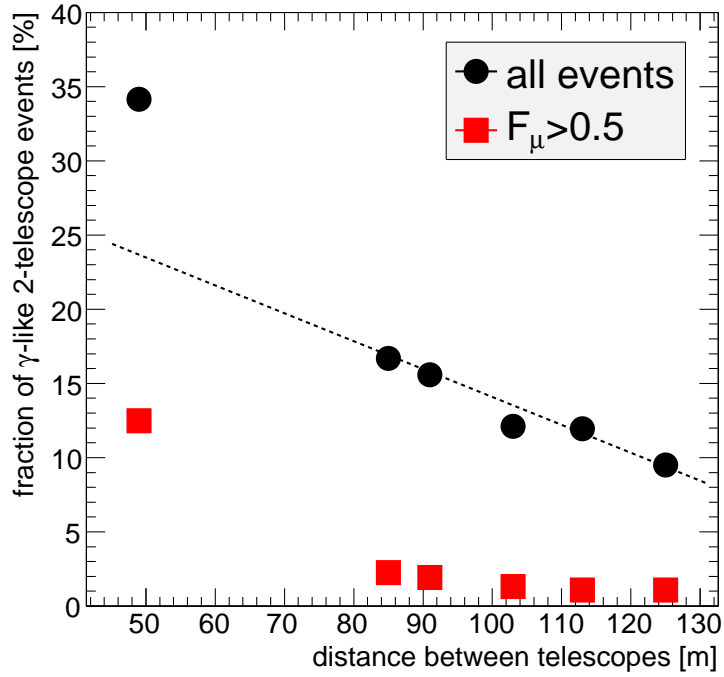


Figure 6: Fraction of  $\gamma$ -like events with a two-telescope array trigger vs. distance between each telescope pair. The dotted line is drawn to guide the eye (QGSJet/FLUKA simulations).



There are several ways to eliminate the majority of these events. The most obvious ones are to modify the trigger condition to use only 2-telescope triggers of pairs with larger distances (e.g. pairings other than Telescope T1+T4) or to require  $> 2$  triggered telescopes. This suppresses muonic events at the trigger level (rejection of 2-telescope triggers on T1+T4 reduces the number of muonic  $\gamma$ -like events by about 40%), but also reduces the sensitivity to primary  $\gamma$ -rays at low energies. Another approach uses the difference in the emission height of the Cherenkov photons [3] of muonic  $\gamma$ -like events and  $\gamma$ -ray showers. The production height of Cherenkov photons from muons (in muonic 2-telescope events) is typically below 2-3 km above ground. In contrast, Cherenkov light from air showers is emitted around the shower maximum at typically 8-10 km height.

The distance  $c$  between the image centroids in the cameras of two telescopes pointing towards the source (parallel pointing mode) is related to the distance  $D$  of the telescopes to each other and the height of the Cherenkov emission maximum  $h$  by  $c = D/h$ . Figure 7 shows the distributions of  $h$ , estimated with this simple relationship for  $\gamma$ -rays and muonic  $\gamma$ -like events. There is a very clear separation between the two distributions, and with a cut at  $h = 4$  km about 80% of all muonic  $\gamma$ -like events can be suppressed, while less than 2% of the  $\gamma$ -ray events are lost.

### 3.2 Pion-induced $\gamma$ -like proton showers

A proton shower is approximately a superposition of many electromagnetic subshowers initiated by the decay of neutral pions, and of muons from the decay of charged pions. The different subshowers produce an irregular Cherenkov photon distribution at the ground, and thus the images of proton showers in the camera of an IACT are usually patchy and broad. This makes most of them easily distinguishable from  $\gamma$ -ray showers. For a  $\gamma$ -like image, a proton shower must either be dominated by one subshower or only one of the subshowers is seen by the telescopes (see example in Figure 4 left). Therefore, in the following, particle production in the early shower development is investigated, and especially those secondary particles which carry a significant part of the primary energy. Events with a 3-fold array trigger are selected to remove all muon-induced events from the simulated event sample.

Figure 8 shows the distribution of secondary particles in the first interaction in proton showers. Only particles with an energy of at least 20% of the primary energy are counted. While the distribution for all simulated events shows the expected ratio of charged to neutral pions of 2 to 1, this ratio approximately reverses for particles in events with a 3-fold array trigger. Well above-average Cherenkov light emission is needed to trigger three or more telescopes. As the large number of  $\pi^0$ 's indicates, the light originates in electromagnetic subshowers initiated by  $\pi^0$  decay. About 50% of all secondaries in the first interactions of  $\gamma$ -like proton showers are neutral pions. The second neutral particle with predominately electromagnetic decay modes is the  $\eta$ -meson. While it constitutes only a very small fraction of secondaries in normal proton showers, a few percent of  $\gamma$ -like events with a 3-fold array trigger contain high energy  $\eta$ 's.

Simulations of  $\gamma$ -induced showers show that an energy of about 80 GeV or more is needed to trigger the array and pass all quality and  $\gamma$ -hadron separation cuts. Similar energies are required too, in the dominating subshower for  $\gamma$ -like proton showers. To investigate this, in the simulations the energy and production height of all  $\pi^0$ 's and  $\eta$ 's with energies above 5 GeV have been recorded. Two variables are examined further, the total energy sum in  $\pi^0$ 's or  $\eta$ 's ( $E_{\Sigma}(\pi^0, \eta)$ ) and the fraction of the primary energy carried away by these particles ( $(E_{\Sigma}(\pi^0, \eta)/E_{tot})$ ). Figure 9 shows the distribution of the distance between the height of first interaction and the  $\pi^0$  production during shower development for events with  $E_{\Sigma}(\pi^0)/E_{tot} > 0.3$ . The figure suggests three categories of events: (i) events with  $E_{\Sigma}(\pi^0, \eta)/E_{tot} > 0.3$  in or close to first interaction, (ii)  $E_{\Sigma}(\pi^0, \eta)/E_{tot} > 0.3$  later during the shower development, and (iii) those events which do not appear at all in the figure ( $E_{\Sigma}(\pi^0, \eta)/E_{tot} < 0.3$  for the whole shower). In this example, about 50% of the relevant particle production occurs in or shortly after the first interaction, about 25% of the events pass this threshold about 5 to 10 km after the first interaction, and 25% of the events never accumulate 30% of their energy in the electromagnetic channel.

The importance of the production of high-energy  $\pi^0$ 's is highlighted in Figure 10 (left and

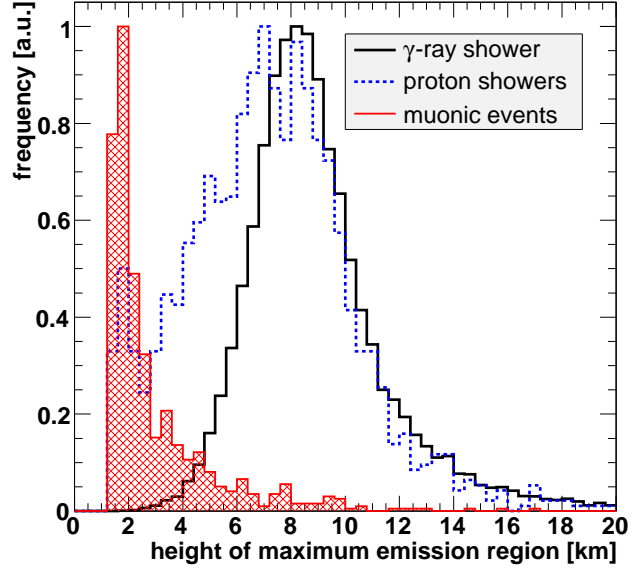


Figure 7: Height of the region of maximum Cherenkov photon emission, calculated from the position of the image centroids in Telescopes 1 and 4 (QGSJet/FLUKA simulations).

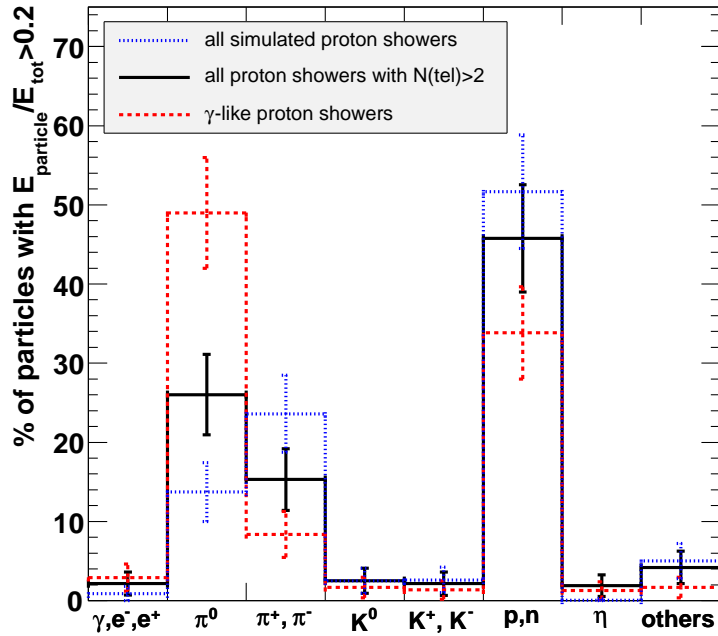


Figure 8: Distribution of secondary particles from the first interaction in proton showers. Only particles with energies larger than 20% of the primary energy are counted (QGSJet/FLUKA simulations).

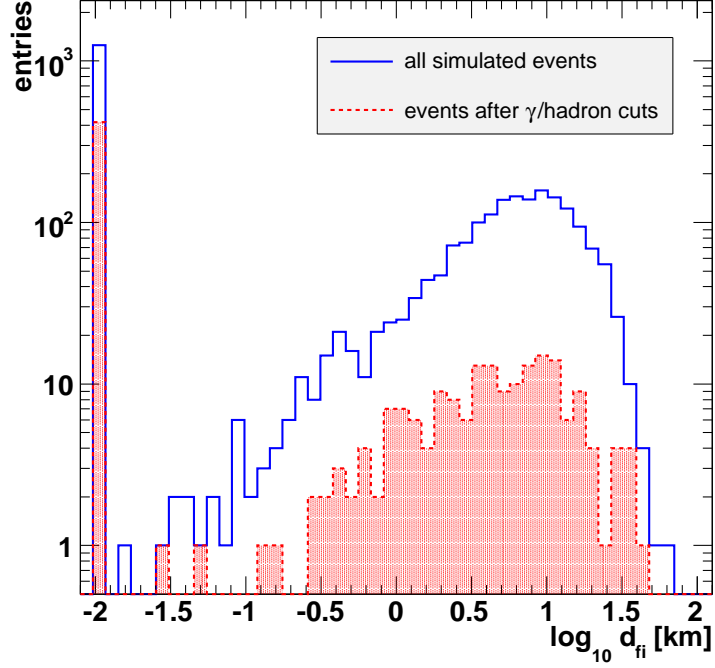


Figure 9: Distribution of distance  $d_{fi}$  between height of first interaction and  $\pi^0$  production during shower development for events with  $E_{\Sigma}(\pi^0)/E_{tot} > 0.3$ . Events with  $d_{fi} < 10$  m are entered in the bin at  $\log_{10} d_{fi} = -2$  (Sibyll/FLUKA simulations).

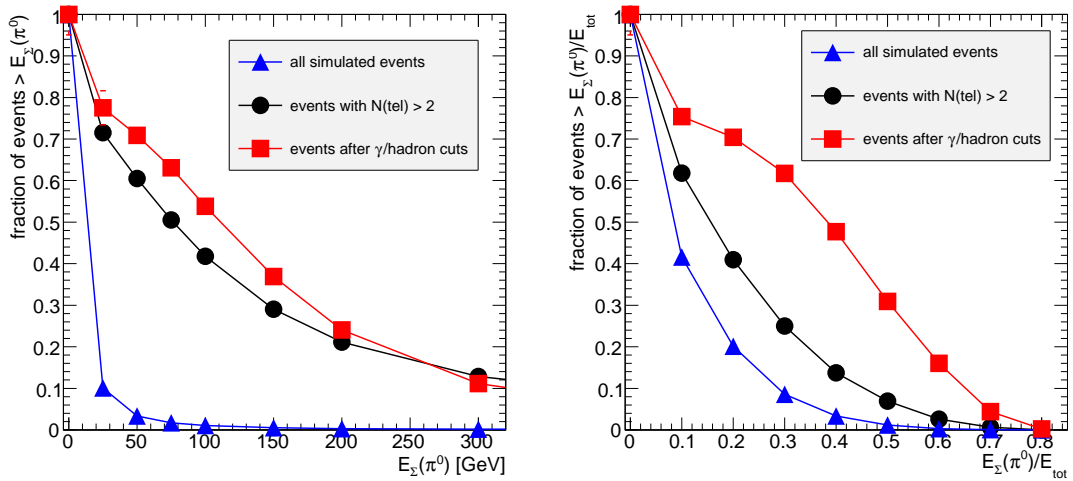


Figure 10: Fraction of events with  $E_{\Sigma}(\pi^0)$  (left) and  $E_{\Sigma}(\pi^0)/E_{tot}$  (right) larger than the value on the abscissa in, or close to, the first interaction ( $d_{fi} < 10$  m). All values for Sibyll/FLUKA simulations.

right). The fraction of events with a  $\pi^0$  energy sum above 80 GeV in all simulated proton showers is very small, while the majority of events with a 3-fold array trigger exceed this threshold.  $\gamma$ -like events are even more likely to contain high-energy  $\pi^0$ 's. The dominance of electromagnetic subshowers in  $\gamma$ -like proton events can be seen in Figure 10 (right). These events are 4-10 times more likely to have an electromagnetic energy share of 40% or more of the primary energy.

Both findings suggest that, firstly, the electromagnetic part in the proton initiated shower has to be energetic enough to trigger the array and, secondly, this part must carry a significant part of the primary energy to prevent the occurrence of other large subshowers that would disturb the  $\gamma$ -like appearance of the Cherenkov image in the cameras.

The fraction of events which do not pass the threshold in the energy sum  $E_{\Sigma}(\pi^0, \eta)$  can be used to accelerate the simulation of background events for IACTs, using a two-pass approach. In a first pass air showers are simulated without any Cherenkov photon production. For CORSIKA this is about 20-100 times faster than simulations with Cherenkov photon production (depending on the Cherenkov photon bunch size parameter). Next, only events which pass a certain  $\pi^0$  and  $\eta$  energy sum threshold, are simulated with Cherenkov photon production, accepting only a small loss in genuine  $\gamma$ -like proton showers. The requirement of  $E_{\Sigma}(\pi^0, \eta) > 30$  GeV, for instance, would reduce the number of fully simulated events by a factor of 9, with a loss of less than 5% of  $\gamma$ -like events (see Figure 11).

Primaries other than protons have so far been neglected in this analysis, although they compose about 25% of all cosmic rays in this energy range. Their contribution to  $\gamma$ -like showers is suppressed because the energy ( $E$ ) of the primary is shared by several nucleons of energy  $E/A$  each. A single nucleon, even if it dumps all its energy into a  $\pi^0$ , can therefore only contribute  $E/A$  to the electromagnetic channel. To get the large fraction of  $E$  (say 80%) required for a  $\gamma$ -like event, many of the nucleons would have to produce almost exclusively  $\pi^0$ s. The nucleons of a primary nucleus interact independently (the typical binding energy is much smaller than their energy). The probability for a nucleon  $p_n$  to produce predominantly electromagnetic secondaries (e.g.  $> 50\%$ ) is already as low as 1% (see Figure 10, right panel). Therefore, the probability of  $A$  nucleons producing all predominantly electromagnetic output scales to first approximation with  $(p_n)^A$ , which is even for Helium of the order of  $10^{-4}$ .

## 4 Influence of interaction models

Results from simulations depend in general on the choice of the nuclear and hadronic interaction model. Models differ since those interactions are not well known in the kinematical regions relevant to cosmic rays (i.e. high energies, very forward emission angles). Therefore, models rely typically on phenomenological descriptions of interactions and extrapolate to the energy and angular ranges required. For the TeV range the extrapolation from collider experiments is still moderate. Nevertheless, particle interactions (cross-sections, energy spectra, multiplicity distributions, etc.) do differ significantly for both low and high energy interaction models (see for example [17], [18], [10], [11]). The CORSIKA package allows the systematic study of these differences since several low- and high-energy interaction models are available in the same framework. The transition energy between high and low interaction models varies from 50 GeV to 1 TeV, depending on the model combination chosen. Here we examine the models FLUKA (version 2003.1) [7], GHEISHA (version 2002) [8], URQMD (version 1.3.1) [4] for low energies, and QGSJet (version 01c) [16] and Sibyll (version 2.1) [6] for high-energy interactions.

Simulations of the interaction of protons with nitrogen nuclei (i.e. the first interaction in a proton-induced air shower) are used to study the amount of energy deposited in the electromagnetic component right at the start of the shower development. Figure 12 shows the distribution of the energy in the electromagnetic component for 100 GeV protons in different interaction models. Figure 13 displays the probability that more than 50% of the primary energy is deposited in the electromagnetic component, as a function of primary energy. Note that not all models cover the whole energy range. QGSJet and Sibyll are not supposed to be used below about 80 GeV primary energy, and GHEISHA is a low energy model, not suitable for energies well above 100 GeV.

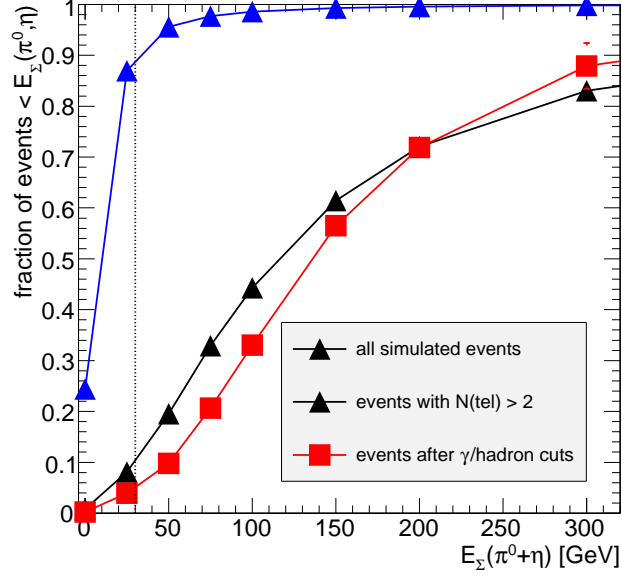


Figure 11: Fraction of events with  $E_{\Sigma}(\pi^0, \eta)$  (sum of energy of all  $\pi^0$ 's and  $\eta$ 's) smaller than the value on the abscissa during the whole shower development. Events with  $N_{tel} \geq 3$  telescopes are selected for this figure (Sibyll/FLUKA simulations).

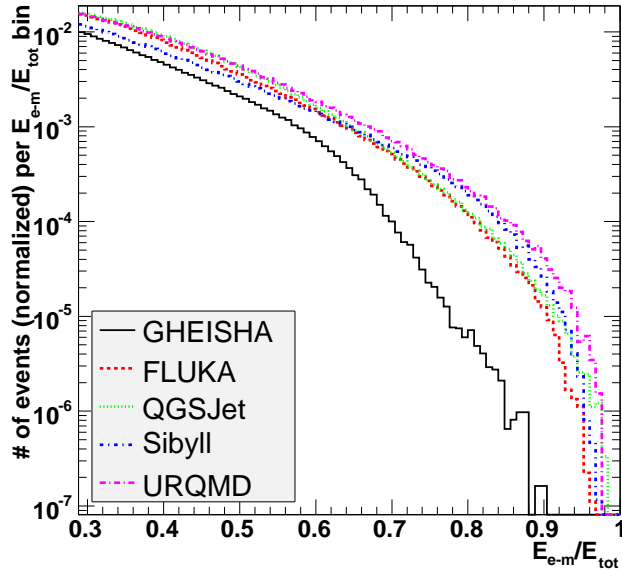


Figure 12: Energy deposited in the electromagnetic components ( $\gamma$ ,  $e^{\pm}$ ,  $\pi^0$ ,  $\eta$ ) in the interactions of 100 GeV protons with nitrogen, for different interaction models. The figure is normalized to the total number of simulated events.

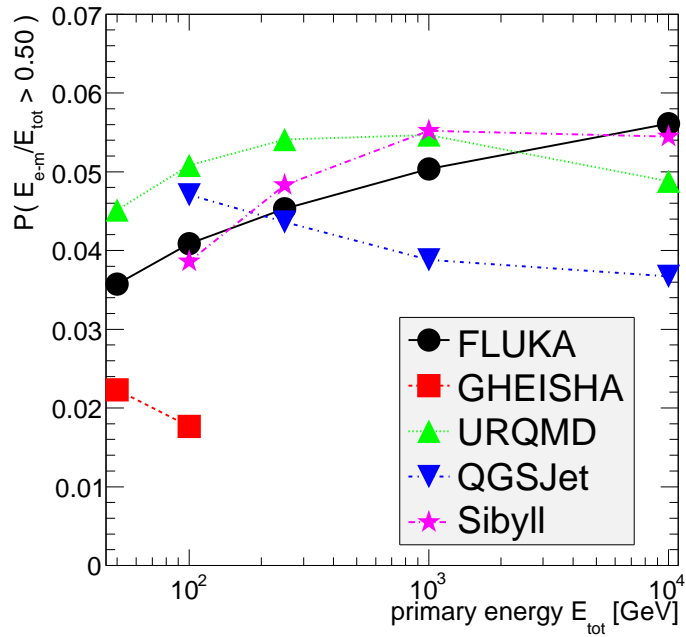


Figure 13: Probability that more than 50% of the primary energy is deposited in the electromagnetic part in proton-nitrogen collisions for different interaction models and primary energies.

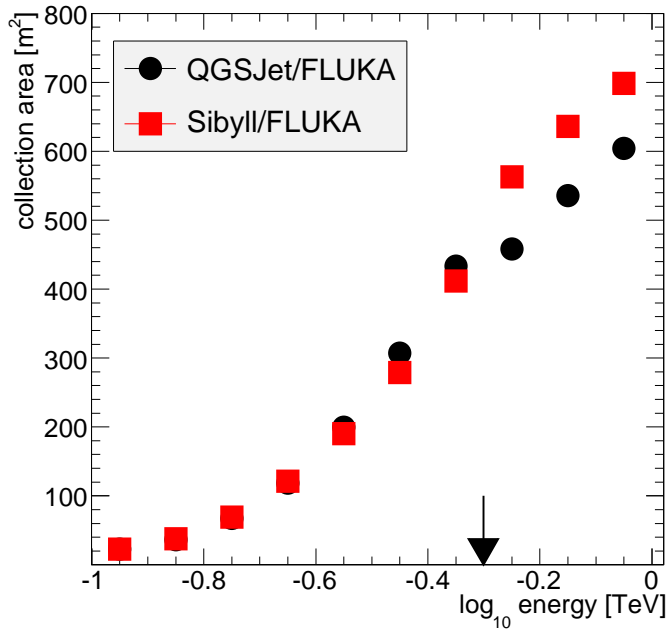


Figure 14: Collection area of the considered array of four telescopes for proton showers for QGSJet/FLUKA (transition energy 500 GeV) and Sibyll/FLUKA (transition energy 80 GeV) simulations. The arrow indicates a primary energy of 500 GeV.

GHEISHA gives a very different prediction compared to other models: events with large  $E_{e-m}/E_{tot}$  are less than half as probable. According to ref. [10], GHEISHA does not reproduce well the available experimental data of pion production and generates in general too few pions. Differences between the other models are in the range of 20-40%. URQMD, Sibyll, and FLUKA tend to deposit more energy in the electromagnetic part, QGSJet systematically less. However, in the past QGSJet was the most successful of the interaction models available, when compared with air shower data. QGSJet employs the most sophisticated treatment of diffractive interactions and produces on average more secondaries than other models. Therefore, it is not surprising that QGSJet finds it more difficult to produce secondaries with large fractions of the primary energy.

What is the effect of these differences on the Cherenkov photon part of the air shower and on the simulated performance of arrays of IACTs? Table 1 shows that the number of reconstructed and selected events of QGSJet/FLUKA and Sibyll/FLUKA simulations are very similar. Also, the fraction of muonic  $\gamma$ -like events differ very little: however, these numbers are a convolution of the primary proton energy spectrum and the energy dependent detection and selection efficiencies of the experiment. Energy dependent measures like the collection area should give a better description of the performance of IACTs. The collection area of an instrument is an overall measure of the number of Cherenkov photons in the shower, their angular and spatial distributions, and the energy dependence of it. It is also affected by the probability and the shape of the images.

The energy dependent collection areas, after all  $\gamma$ -hadron separation cuts, of QGSJet/FLUKA and Sibyll/FLUKA simulations are compared in Figure 14. Note that the transition energy for the QGSJet/FLUKA simulations is at 500 GeV, for Sibyll and FLUKA it is at 80 GeV (and that also lower energy interactions play a role in the shower development of high energy showers). The collection areas are very similar in the energy range from 100 GeV to 500 GeV, where the figure shows essentially a comparison of pure FLUKA with Sibyll/FLUKA simulations. However, the QGSJet/FLUKA collection area ( $> 500$  GeV) shows a discontinuity exactly at the transition energy between QGSJet and FLUKA, with a smaller collection area at higher energies. As shown in Figure 13, the difference in the amount of energy between QGSJet, and FLUKA at 500 GeV deposited into the electromagnetic part of the shower is about 15-30%, while the difference between Sibyll and FLUKA is below 5%. This QGSJet version, in contrast to Sibyll and FLUKA, cannot reproduce the experimental values of pion multiplicity in proton-proton interactions at energies of about 500 GeV [10]. A very similar analysis of events with a primary energy less than 100 GeV shows that the GHEISHA model predicts about 20% less  $\gamma$ -like proton events with 3-fold array triggers. Interestingly, the number of two-telescope events due to muons increases by about the same amount. The systematic differences of about 25% in the predictions of Sibyll/FLUKA and QGSJet/FLUKA at energies above 500 GeV for the collection area translate directly into an uncertainty of about 10% for any sensitivity estimate. QGSJet/FLUKA predicts a lower background, and therefore a higher sensitivity to  $\gamma$ -ray sources. The choice of transition energies in this study does not allow a definitive statement about the differences between QGSJet and Sibyll at energies below 500 GeV, but Figure 13 indicates that both models converge at about 200 GeV and give here results similar to FLUKA.

Both findings, the different collection area of QGSJet at energies above 500 GeV and the shortcomings of GHEISHA, indicate that a careful choice of both, interaction models and transition energies, is necessary to obtain reliable results.<sup>1</sup>

## 5 Summary

With available simulation tools, air showers of primary  $\gamma$ -rays and cosmic rays, and complex telescope systems can be modeled in sufficient detail to study the design and performance of current and future imaging atmospheric Cherenkov telescope systems.

---

<sup>1</sup>During completion of this paper a new version of QGSJet has been released, with marked improvements in the sub TeV range. [24].

$\gamma$ -ray shower simulations in the GeV - 100 TeV range have very small uncertainties, as the relevant physics is well known. On the basis of these simulations  $\gamma$ -ray selection procedures are optimized and  $\gamma$ -induced showers can be securely identified.

The dominant background, however, is due to cosmic rays, and some cosmic ray showers look very much like  $\gamma$  showers. Simulations reveal which type of background events trigger the instruments and survive all  $\gamma$ -hadron selection cuts. They are mainly hadronic events which, by chance, transfer much of the primary's energy to electromagnetic subshowers during the first few interactions. Thus, interactions with low multiplicity and high  $\pi^0$  fraction are the most important, and pose an irreducible background. These showers are mainly produced by diffractive interactions with particle production in the very forward region, and because diffractive events are subject to considerable model uncertainties, the cosmic-ray background can only be estimated with about 20-40% uncertainty, based on current models.

Events with energetic muons can produce  $\gamma$ -like images, even in stereoscopic systems, if the telescopes are close enough to be within the Cherenkov lightpool of the muon. However, a cut in the distance between the image centroids normalised by the telescope distance removes these events efficiently.

The preselection of showers with a high energy fraction in electromagnetic particles can be used to reduce overall computing time for background calculations by approximately an order of magnitude.

## Acknowledgments

G.M. acknowledges the support as a Feodor Lynen Fellow of the Alexander von Humboldt foundation. He would also like to thank the High Energy Astrophysics Group of the University of Leeds for hospitality during the main phase of this work.

## References

- [1] F. Aharonian et al. (H.E.S.S. Collaboration), *Science* 307 (2005) 1938
- [2] F. Aharonian et al. (H.E.S.S. Collaboration), *Science* 309 (2005) 746
- [3] F. Aharonian et al., *Astroparticle Physics* 6, (1997) 343
- [4] S.A. Bass et al., *Prog. Part. Nucl. Phys.* 41 (1998) 225  
M. Bleicher et al., *J. Phys. G: Nucl. Part. Phys.* 25 (1999) 1859; <http://www.th.physik.uni-frankfurt.de/~urqmd/>
- [5] C.Duke & S.LeBohec, <http://www.physics.utah.edu/gammaray/GrISU/>
- [6] R. Engel et al., *Proc. 26<sup>th</sup> Int. Cosmic Ray Conf.*, Salt Lake City (USA) 1 (1999) 415
- [7] A. Fassò et al., *FLUKA: Status and Prospective of Hadronic Applications*, Proc. Monte Carlo 2000 Conf., Lisbon, Oct. 23-26, 2000,  
A. Kling, F. Barao, M. Nakagawa, P. Vaz eds., Springer (Berlin) 955 (2001); <http://www.fluka.org/references.html>
- [8] H. Fesefeldt, Report PITHA-85/02 (1985) RWTH Aachen
- [9] D. Heck et al., Report FZKA 6019, Forschungszentrum Karlsruhe (1998)
- [10] D. Heck *Nucl. Phys. B (Proc. Suppl.)* 151 (2006) 127
- [11] D. Heck, VIHKOS CORSIKA SCHOOL 2005  
<http://www-ik.fzk.de/corsika/corsika-school/program.htm>



- [12] D.Heck, private communication (2005)
- [13] A.M. Hillas, Proc. 19th Int. Cosmic Ray Conf., 3 (1985) 445
- [14] A.M. Hillas, Astrophysical Journal 503 (1998) 744
- [15] W. Hofmann, Astroparticle Physics 12 (1999) 135
- [16] N.N. Kalmykov et al., Nucl.Phys. B (Proc. Suppl.) 52B (1997) 17
- [17] J. Knapp et al., Report FZKA 5828 (1996), Forschungszentrum Karlsruhe
- [18] J. Knapp, Nucl. Phys. B (Proc. Suppl.) 75A (1999) 89
- [19] F.X. Kneizys et al., *The Modtran 2/3 report and lowtran 7 model*, Technical Report, Ontar Corporation (1996)
- [20] H. Krawczynski et al., Astroparticle Physics 25 (2006) 380
- [21] G. Maier et al., *Monte Carlo Studies of the first VERITAS telescope*, 29th ICRC, Pune (2005)
- [22] National Aeronautics and Space Administration (NASA), U.S. Standard Atmosphere 1976, NASA-TM-X-74335, (1976)
- [23] W.R. Nelson et al., Report SLAC 265 (1985)
- [24] S.S. Ostapchenko, Nucl. Phys. B (Proc. Suppl.) 151 (2006) 143 and 147  
preprint hep-ph/0412332 (2004) and hep-ph/0501093 (2005)
- [25] G. Schatz, Space Science Reviews 75 (1996) 71
- [26] T. Weekes et al., Astroparticle Physics, 17 (2002) 221